Journal of the Meteorological Society of Japan

EARLY ONLINE RELEASE

The DOI for this manuscript is
DOI:10.2151/jmsj.2025-010
J-STAGE Advance published date: January 14, 2025
The final manuscript after publication will replace the preliminary version at the above DOI once it is available.

Analysis of Tropical Cyclone Rapid Intensification in the Southwest Pacific Region

Edward MARU

Forecasting section, Solomon Islands Meteorological Service, Honiara, Solomon Islands

Graduate School of Engineering and Science, University of the Ryukyus, Nishihara, Japan

Disaster Prevention Research Institute, Kyoto University, Uji, Japan

Kosuke ITO

Disaster Prevention Research Institute, Kyoto University, Uji, Japan

Typhoon Science and Technology Research Center, Yokohama National University, Yokohama, Japan

Hiroyuki YAMADA

Department of Physics and Earth Science, University of the Ryukyus, Nishihara, Japan

Revision submitted to the *Journal of the Meteorological Society of Japan*

15 November 2024

---

* Corresponding author: Kosuke Ito, *Kyoto University, Uji, Japan*

Email: ito.kosuke.2i@kyoto-u.ac.jp

Tel: +81-774-38-4159

Fax: +81-774-38-4158

Abstract

This study statistically investigates the characteristics of tropical cyclones (TCs) undergoing rapid intensification (RI) in the Southwest Pacific (SWP) region in the 37 years from 1986 to 2022. Among 364 TCs, 82 rapidly intensifying TCs (RI-TCs) were defined as TCs that experienced maximum wind speed increase of 30 kt (15.4 $\mathrm{m\,s^{-1}}$) or more in a 24-h period. RI-TCs are frequently observed over the zonally elongated area around coral sea, south of Solomon Islands (Solomon Sea), Vanuatu, Fiji, Tuvalu, Tokelau and Samoa, while RI-TCs were rarely observed in areas of Tasman Sea, Tonga, northern waters of New Zealand, Cook Islands, Niue and French Polynesia. RI-TCs preferentially occur during the southern hemisphere summer season. Frequency of RI-TC occurrence shows a slowly increasing trend over the 37-year period. However, this increasing trend was not statistically significant at the 95% confidence level. In El Niño years, TCs tend to undergo RI more frequently presumably due to the average genesis to the further north where sea surface temperature (SST) and ocean heat content were high. In contrast, RI-TCs occurred less frequently during La Niña years. The RI onset typically occurs 0–42 h after TC genesis with a peak frequency observed just after genesis (0–6 h). The RI duration is usually 1–2 days with a peak at 24 hours. The mean lifetime of RI-TCs lifetime was 7.86 days, longer than that of non-rapidly intensifying TCs (NR-TCs) (3.72 days). In terms of average intensity, RI-TCs have significantly lower lifetime central pressure and higher lifetime maximum wind speed than NR-TCs. RI-TCs

tend to develop into more severe TCs as a result of formation in environments favorable for TC development such as weak vertical wind shear, deep moist layer, high SST and TC heat potential.

Keywords: tropical cyclone; rapid intensification; El Niño Southern Oscillation; Southwestern Pacific; global warming

1. Introduction

The Southwestern Pacific (SWP) region consists mainly of small Island nations including the neighboring continent of Australia and has approximately 10 tropical cyclones (TCs) annually. The islands are isolated with some low-lying geographical settings making the region extremely vulnerable to intense TCs. One of the great challenges for disaster prevention associated with intense TCs is the prediction of rapid intensification (RI) (Rappaport et al. 2012; Smith et al. 2015; Ito 2016). Accurate timing is hard to forecast which may lead to large intensity forecast errors. In terms of disaster preparedness and mitigation, accurate intensity forecasts are crucial for impact information through an early warning system, which is a global activity that governs countries, governments and individuals to understand the forthcoming hazardous weather and disaster plans to minimize impeding impacts from TC-related storm surges, heavy rainfall, and violent winds such as Disaster Risk Reduction (https://community.wmo.int/en/activity-areas/drr; Obasi 1994) within the framework of World Meteorological Organization (WMO).

Considering the severity of extreme TCs in the region, the threat might be aggravated due to the influence of global warming on the increasing rate of RI-TCs. Recent studies over other basins have indicated the increasing number in RI-TCs. Bhatia et al. (2019) showed a detectable increase rate of intensification over the Atlantic basin with a positive contribution from anthropogenic forcing. Bhatia et al. (2022) gave a potential explanation for the global increase in TC RI is due to thermodynamics around TCs and the positive contribution from anthropogenic warming. The rates of RI-TC occurrence in the western North Pacific (WNP) have increased from the 1990s to the late 2000s according to RSMC Tokyo best track (Ito 2016; Fudeyasu et al. 2018), while Shimada et al. (2020) revealed that the increase in RI events seen in best track data for the WNP was mainly due to procedural changes at Japan Meteorological Agency (JMA). Balaguru et al. (2018) revealed that the RI magnitude had increased in the central and eastern tropical Atlantic basin during the period of 1986-2015. A better understanding and representation of actual TC wind speed and its tracks leads to a better representation of the impact information (Takemi 2018).

An earlier study of RI by Kaplan and Demaria (2003) showed large-scale characteristics of TCs undergoing RI (RI-TCs) in the North Atlantic. Kaplan et al. (2010, 2015) also examined large-scale characteristics for the Atlantic and eastern North Pacific basins. Several aspects associated with RI events have been identified from observational and modelling, which include organization of eyewall convection and the associated mesoscale vortices (Eastin et al. 2005; Kieper and Jiang 2012), high ocean heat content (Shay et al. 2000; Bosart et al. 2000; Wada and Usui 2007; Lin et al. 2008; Fudeyasu et al. 2018), and large-scale environmental conditions such as strong mid-level inflow and upper-level outflow, low vertical wind shear (VWS) or lower tropospheric high relative humidity (Kaplan and DeMaria, 2003; Molinari and Vollaro, 2010; Kieu et al. 2014; Fudeyasu et al. 2018).

These results are consistent with the basic understanding of TC intensities. The ocean is an enormous heat reservoir and even TCs cannot deplete it during its pass over

(Emanuel 2005). Nevertheless, it was proposed that TCs cool the sea surface temperature (SST) by producing turbulent mixing or upwelling (Price 1981), and the large ocean heat content contributes to RI by reducing the magnitude of TC-induced cooling at sea surface (Lin et al. 2005; Wada 2015). Areas with largest increase in SSTs and potential intensities are collocated with increasing positive changes in intensification rates (Emanuel 1999). As for the atmospheric component, VWS has been known to inhibit the symmetric structure of a TC and weaken the TC intensity (e.g., Frank and Ritchie 2001), and deep humid air is prerequisite condition for the deep convection in a TC (e.g., Nasuno et al. 2016).

The above-mentioned studies generally addressed the characteristics and trends of RI-TCs in the basins and regions other than SWP. However, it is important to make sure that similar tendencies are also robust and consistent in the SWP for the purposes of disaster preparedness and decision making. Bhowmick et al. (2023) investigated classification analysis of SWP TC intensity changes prior to landfall, but they did not show the annual changes, distribution and characteristics of RI-TC activity in the SWP. Several recent studies done for the SWP TCs focused only on characteristics such as genesis, climatology, variability and general intensification trends within the SWP (e.g., Vincent et al. 2011; Chand and Walsh 2010; Nakano et al. 2017; Maru et al. 2018; Takemi 2018; Tauvale and Tsuboki 2019; Tu'uholoaki et al. 2022; Haruhiru et al. 2022). However, the statistical characteristics of RI-TCs around the SWP region have never been investigated according to the authors' knowledge. Therefore, it is important to describe RI-TC activity over the SWP.

The main objectives of this study are (1) to examine the distribution and annual changes in RI-TC activity (e.g. if RI occurrence trend has increased or not) over the 37 years from 1986 to 2022 and (2) to investigate the characteristics of RI-TCs associated with the large-scale environmental parameters that influence RI, including both atmospheric and oceanic features.

The structure of this paper is as follows: Section 2 describes the data and methodology, Section 3 describes the results (climatology and interannual variation of RI-TCs, duration and distribution of RI events, statistical characteristics of RI-TCs and environmental parameters around RI-TCs), Section 4 is the discussion. Finally, Section 5 is comprised of a conclusion summarizing the findings of the study.

2. Data and Method

This study is based on the Southwest Pacific Enhanced Archive for Tropical cyclones (SPEArTC) best track (BT), which is a six-hourly dataset from 1986 to 2022, as described by Diamond et al. (2012). We obtained these datasets from the Asia-Pacific Data-Research Center (APDRC) (available at https://apdrc.soest.hawaii.edu/projects/speartc/download_speartc.php, accessed on 22 November 2022).

The maximum wind speed (Vmax) is defined as the maximum value of a 10-minute sustained wind at 10-m height. For this study, a TC is defined as a tropical storm that achieved Vmax of ≥ 34 knots (~17 m/s).

For this dataset, the Fiji Meteorological Service serves as the Regional Specialized Meteorological Centre (RSMC) Nadi, and the Australian Bureau of Meteorology (BoM) serves as the Tropical Cyclone Warning Centre (TCWC) Melbourne. When a TC center was located to the east (west) of 160°E, the RSMC Nadi (TCWC Melbourne) dataset was used. In general, best track data between 160°E and 120°W belongs to RSMC Nadi and between 135°E–160°E belongs to BoM. In 2020, the Australian BoM decided to merge the three Areas of Responsibilities of TCWC Brisbane, TCWC Darwin and TCWC Perth in a single Area of Responsibility named TCWC Melbourne. Prior to 2020, the responsibility west of 160° E belongs to TCWC Brisbane. This split follows the framework of World Weather Watch program of the World Meteorological Organization (WMO). We used data from TCWC Wellington instead of RSMC Nadi until December 1992 due to data availability. During June 1995, the Fiji Meteorological Service's Nadi — Tropical Cyclone Centre, was designated as an RSMC by the WMO and prior to that TCWC - Wellington/New Zealand Met Service, Ltd was responsible for RSMC Nadi’s area of responsibility.

The TCs considered are those originated from the area between 5°S–35°S and 135°E–120°W (hereafter, we call it the study domain) (inner rectangular black box in Fig. 1). We tracked an incipient vortex whose intensity category is a tropical depression (TD) from first location recorded in the BT generated within the study domain and considered an RI event even after the tracked TC that underwent the RI outside the study domain in the Southeast Indian Ocean (SEI) and western Australia waters (Figure 1c). TDs were not investigated if they are generated in the study domain but never attained TC status.

An RI event is defined as an increase in maximum wind speed of 30 kt (15.4 $\mathrm{m\,s^{-1}}$) or more in a 24-h period (Fig.2). A rapidly intensifying TC (RI-TC) is defined as the TC that experiences RI, at least once in its lifetime, while a non-rapidly intensifying TC (NR-TC) is defined as the TC that did not experience RI. The frequency distributions of 24-h intensity changes of all TCs investigated is shown in Fig. 3. In total, 364 TCs were examined, and 82 RI events identified. As mentioned earlier, we considered a TD within the study domain that developed into a TC outside the domain. Amongst all the RI-TCs, 6 TDs experienced the RI outside the study domain (Figure 1a). They did not affect our main conclusions.

In this study, each successive period satisfying the RI definition was counted as one "RI event." This definition is the same as that used by Shimada et al. (2020). It was possible for a TC to experience two or three events during its lifetime. We define the RI onset as the beginning of the initial RI event (Fig.2). The duration of RI is from the RI onset to end time of RI. The end time of RI event corresponds to the time at which development rate no longer satisfying criteria of RI definition after the final RI event. During the lifetime of each TC, TC genesis time is defined as the time in which a tropical low achieved Vmax of ≥34 knots (~17 m/s), and TC mature time corresponds to the time when a TC archives its lifetime maximum intensity. TC decay time refers to the last time at which the maximum intensity of a disturbance (including the period after the transition to an extratropical cyclone (ETC) or a subtropical cyclone) is below 34 knots (~17 m/s) (Fig.1).

The conventional two-tailed *t*-test (95% significances) was used to check if the general characteristics of TC and environmental physical parameters between RI-TC and NR-TC and the climatological tendency are statistically significant. The statistical test for statement on the long-term trend was checked with the slope of the regression line. We call these results “significant” if the confidence level is over 95%. Statistical characteristics, such as location (average latitude and longitude), intensity (average maximum wind speed and central pressure), development duration from genesis time to mature time, and lifetime from genesis time to decay time were derived from the BT data. The monthly El Niño Southern Oscillation (ENSO) indexes were obtained from BoM (available at http://www.bom.gov.au/climate/enso/soi/, accessed on 30 October 2024). The definition of ENSO state for each year in this study is based on the yearly mean of Southern Oscillation Index (SOI) from January to December. A yearly mean SOI below −7 is classified to an El Niño year, while that above +7 is classified to a La Niña year. The specific humidity, air temperature, geopotential height, zonal and meridional wind datasets were taken from the Japanese 55-year Reanalysis (JRA-55; Kobayashi et al. 2015) (details available online at http://jra.kishou.go.jp/JRA-55/index_en.html).

JRA-55 is a 6-hourly dataset with a horizontal resolution of 1.25° for both longitude and latitude. As for oceanic data, SST was taken from the delayed model version of Merged Satellite and in-situ data Global Daily Sea Surface Temperature (MGDSST) (Kurihara et al. 2006) and TC heat potential (TCHP) was taken from Japan Agency for Marine-Earth Science and Technology (JAMSTEC), Japan Coastal Ocean Predictability Experiments-Forecasting Global Ocean (JCOPE-FGO) (Kido et al., 2022).

We calculated statistical summaries and significant differences between RI-TCs and NR-TCs in the following physical parameters: magnitude of VWS, atmospheric relative humidity, SST and TCHP (1) within the radius of 300 km and (2) within an annulus of 200–800 km from the TC center.

Here, VWS is defined as the magnitude of deep-layer horizontal wind vector difference between 850 hPa and 200 hPa as follows:

$$\mathrm{VWS} = \sqrt{(\mathrm{U}_{200} - \mathrm{U}_{850})^2 + (\mathrm{V}_{200} - \mathrm{V}_{850})^2} \quad (1)$$

TCHP was calculated by summing the ocean temperature deviation relative to 26°C from the surface to the depth of the 26°C isotherm (Leipper and Volgenau 1972; Wada 2015), as follows:

$$Q = C_p \sum_{i=i26}^{i=1} \rho_i (T_i - 26) \Delta z_i \quad (2)$$

where Q is TCHP ($\mathrm{kJ/cm^2}$), C_p is specific heat (4,184 kJ/kg/K) of sea water at constant pressure, T_i is sea water temperature (℃) at *i*th level, Δz_i is layer thickness (m) possessed by the *i*th level, i26 is the layer number with ocean temperature 26℃, and ρ_i

is the density of sea water at the *i*th level. If the SST is below 26℃, TCHP is set to zero. The lower and mid-tropospheric relative humidities were respectively calculated in atmospheric layers between 850-700 hPa (RHLO) and 700-500 hPa (RHMD) using Tetens' equation from specific humidity, air temperature and pressure.

3. Results

3.1. Climatological and interannual variation of RI-TC

Among the 364 TCs analyzed over the 37-yr period 1986 to 2022, 82 RI-TCs (22.5% of the total) and 282 NR-TCs were detected using the definition employed in this study. Figure 1 shows distribution of RI genesis. The number of RI-TC occurrences was 7, 70, and 5 in the latitudes of 6°S–10°S, 10°S–20°S, and 20°S–35°S, respectively. The onset of RIs was most frequently observed over the zonally elongated area around coral sea, south of Solomon Islands (Solomon Sea), Vanuatu, Fiji, Tuvalu, Tokelau and Samoa. In contrast, the onset of RIs was rarely observed in areas of Tasman Sea, Tonga, northern waters of New Zealand, Cook Islands, Niue and French Polynesia. This study defined RI zone as at longitudes of 145°E –160°W latitudes of 8–20°S. RI-TCs over the study domain are concentrated within 8°S–20°S (Fig. 1).

Figure 4 shows the monthly distribution of RI-TCs. A large variability in seasons is seen among the number of RI-TCs. They preferentially occurred during the SWP cyclone season from November to April. This seasonal variability is due to the seasonal variation among all TC occurrences. The most frequent number of RI-TC occurrences was seen in March with 21 RI-TCs followed by 19 and 18 RI-TCs in February and January, respectively.

The annual number of RI-TCs over the SWP shows the slowly increasing trend (+0.03 per year) from 1986 to 2022 (Fig. 5a). Similar increasing trend in RI-TC events were also described in the results by previous studies (Fudeyasu et al. 2018; Ito 2016; Shimada et al. 2020) for the Northwest Pacific (NWP) and Kranthi et al. (2023) for the Arabian sea of North Indian Ocean. However, this increasing trend was not statistically significant at the 95% confidence level based on a regression analysis (Fig. 5a). In contrast, the annual number of all TCs (RI-TCs and NR-TCs) decreased at a rate of -0.04 per year in the same period (Fig. 6). The decreasing trend in the annual number of TCs was also not statistically significant at the 95% confidence level based on the regression analysis as consistent with Tauvale and Tsuboki (2019), who investigated characteristics of TCs in the SWP for 48 TC seasons (1969/1970–2016/2017).

Slowly increasing number of RI-TCs and decreasing number of all TCs result in the increase of RI-TC occurrence rates, particularly after 2016 (Table 1). Ito (2016) reported that the RI-TC occurrence rate had nearly doubled in the past 25-yrs over the WNP region. It should be cautioned that the increasing trend is not necessarily due to climatological changes. Shimada et al. (2020) stated that the increase in RI event seen in RSMC Tokyo best track data for the WNP was mainly due to procedural changes at JMA and qualitative changes related to observational techniques. (e.g. JMA started using microwave satellite imagery in 2006). For TCs in the SWP, “BoM first started using microwave satellite imagery around 2001, but the application varied until about 2003 or 2004 when there was more training and understanding, whereas RSMC Nadi started microwave satellite imagery in 2010” (personal communication with Joe Courtney in BoM, May 9, 2024). The increasing rate of RI-TCs relative to NR-TCs could be from the impact of climate change but it can also result from the procedural changes. This topic should be more elaborated in the future works.

Figure 5a indicates that RI-TCs occurred most frequently in 2018, followed by 5 RI-TCs in 2005. In contrast, only one RI-TC was observed in 1988, 1990, 1995, 1999, 2001,2002, 2009, 2021 and 2022. Whereas no RI-TC was recorded in 1996 and 2008.

It is possible that the ENSO results in the annual variability in the number of RI-TC occurrences. Figure 5b shows the number of RI-TCs formed based on the yearly ENSO index. The years from 1986 to 2022 were divided into 16 El Niño, 11 La Niña and 10 neutral years. The average number of RI-TCs was 2.6 per year and the average occurrence rate was 24.8% during El Niño years, whereas there were 2.0 and 21% in La Niña years. In neutral years, the number of annual occurrences was 1.9 with the occurrence rate of 20.2% per year (Fig. 7). Thus, TCs in an El Niño year tended to undergo RI more frequently than La Niña and neutral years.

3.2 Duration and distribution of RI events

Figure 8a reveals the RI onset time since genesis time. The RI onset frequency at 0–6 h after time of genesis showed the highest peak (46% of the total), followed by 36–42 h (15%) and 24–30 h (13%). The RI onset occurred more than 3 days after the genesis was very rare. Figure 8b presents the distribution of the RI duration between RI onset and RI end time. The most frequent duration (27% of the total) was the 24-h, followed by the 30-h (19%), 36-h and 42-h (18% each). Therefore, the number of RI decreased as the RI duration increased. It is interesting to note that although there was no RI-TC with an RI duration after 84-h, one event (TC Winston 2016) attained RI duration of 114-h by two RI events. According to Terry and Lau (2018), severe category 5 TC Winston was first noted as a TD on the 07^{th} of February 2016 to the northwest of Vanuatu by RSMC Nadi. The system attained gale force winds (≥35 knots) on the 11^{th} of February 2016 and was named Winston. TC Winston devastated Fiji during its peak intensity, maximum sustained winds of 150 kt and central pressure of 884 hPa on the 20^{th} of February 2016.

3.3 Statistical characteristics of RI-TCs

a. Intensity

It is important to compare the statistical characteristics of RI-TCs with those of NR-TCs at the genesis time, mature time and decay time. At the genesis time, there were no significant differences in the average intensities of RI-TCs and NR-TCs by definition, but the average intensities were significantly different at mature time. The maximum sustained wind speed (central pressure) of RI-TCs was significantly higher (lower) than NR-TCs at mature time (Table 2). This reflects that RI-TCs tended to develop into intense TCs.

To verify the tendency of an intense TC to develop, we also examined the occurrence of specific categories of TC intensity, using the Australian BoM intensity scale. During the 37-yr analysis period, weak TCs are classified as TCs in the category 1 [34–47 kt (63–88 km/h)] or category 2 [48–63 kt (89–117 km/h)] whereas severe TCs are those in the category 3 [64–85 kt (118–157 km/h)], category 4 [86–107 kt (158–198 km/h)], or category 5 [>107 kt (198 km/h)]. The numbers of TCs are 59 in category 3, 54 in category 4 TCs, and 31 in category 5 TCs. The occurrence rates RI-TCs and NR-TCs were divided by the number of occurrences for severe and weak TCs, similar to Fudeyasu et al. (2018). Among all severe TCs detected, there were 62 NR-TCs and 82 RI-TCs. The occurrence rate of RI-TCs among all severe TCs was (57%) greater than that of NR-TCs (Fig. 9). All weak TCs are NR-TCs by definition. Hence, all RI-TCs detected in this study developed into severe TCs. These results are consistent with those of a previous study by Kaplan and DeMaria (2003) over the Atlantic, Fudeyasu et al. (2018) over NWP in which most category 4 or 5 hurricanes were found to undergo RI.

b. Location and lifetime of RI-TCs

To determine the differences between RI-TCs and NR-TCs lifetime and duration, we examine the locations at genesis time, mature time and decay time. The average latitude of

TC formation at genesis time is significantly different between RI-TCs and NR-TCs (Table 2). On average, RI-TCs tend to form significantly more northward (13.32°S) than NR-TCs (15.96°S). Based on the average longitudes, RI-TCs (166.41°E) tend to occur a little further west than NR-TCs (169.20°E) at genesis time. On the other hand, the average longitudes at decay time shows RI-TCs (longitude 177.23°E) tendency to track farther south-eastwards compared to NR-TCS (longitude 174.80°E) (Fig. 3b and Table 2). Because the variation in the longitude at the genesis or maturity is large, the longitudinal difference between RI-TCs and NR-TCs was not statistically significant at both genesis time and decay time.

We considered two measures of TC duration: one is for the development stage from genesis time to mature time, and the other is for the lifetime from genesis time to decay time. The mean duration of the development stages of RI-TCs was 3.6 days, longer than that of NR-TCs (1.62 days). The longer mean duration of the development stages of RI-TCs was partly due to their tendency to form farther north. Similarly, the lifetime was significantly different. Table 2 reveals that the mean duration of RI-TCs lifetime (7.86 days) was much longer than that of NR-TCs (3.72 days).

c. Environmental physical parameters around RI-TCs and NR-TCs

In the following section, we compare the characteristics of environmental physical parameters between RI-TCs and NR-TCs. To explain the differences between RI-TCs and NR-TCs, oceanic and atmospheric environmental parameters around the TC center were calculated in two regions. First, we calculated an annulus average of 200–800 km, and the second method is an area average within 300 km from the TC center. The intensity-SST relationship plays a key role in determining RI-TC occurrence. Figure 10a shows a broad region of high SST (~26–28°C) along latitudes of 0°–22°S and extends eastwards up to 120°W. This region coincides and overlaps with higher TCHP (Fig. 10b). Table 3 shows the average oceanic environmental parameters at the genesis time, mature time and decay time. As shown in Table 3, the oceanic environmental parameters are significantly different between RI-TCs and NR-TCs at genesis time, mature time and decay time; TCHP and SST are higher in RI-TCs. These results are consistent with those of previous studies, indicating that RI-TCs are generated around higher upper ocean heat content (e.g., Hong et al. 2000; Shay et al. 2000; Cione and Uhlhorn 2003; Lin et al. 2005, 2008; Wu et al. 2007; Wada 2015; Fudeyasu et al. 2018 and Kranthi et al.2023). Particularly, the difference of TCHP between RI-TCs and NR-TCs is very significant. According to Wada (2007), TCs intensify rapidly when the TCHP is above 120 $\mathrm{kJ\ cm^{-2}}$. Figure 10b reveals that TCHP is high (~ 50–175 $\mathrm{kJ\ cm^{-2}}$) south of the equator within the study domain, in particular, the TCHP around the Solomon Islands, Vanuatu, Samoa and northern regions of Fiji and Tonga. There are lesser amounts of TCHP (~ 50–75 $\mathrm{kJ\ cm^{-2}}$) in the Coral Sea and the southern waters of Vanuatu and Fiji (Fig. 10b).

On the other hand, SST and TCHP are lower in RI-TC cases during decay time. This result explains that RI-TCs have tracked poleward interacting with cooler waters to the farther south transitioning into ETC. This is consistent to the RI-TC's longer lifespans demonstrated by result in the previous section. It is interesting to note that average SST and TCHP are higher closer to RI-TC center (300 km) annular ring than the outer ring (200–800 km) (table 3). The smaller values with a 200–800 km annulus demonstrated at decay time is consistent to ETC transitioning region due to cold subsurface water located in the south. Figure 10f and 10g shows the geographical difference between RI-TCs and NR-TCs and the difference is not large. The result in the large scale implies that the RI-TC distribution (Fig. 1a) is attributed to favorable basic state, especially in the north of the study domain (Fig. 10a and Fig. 10b).

Next, we examine the atmospheric environmental physical parameters around RI-TCs and NR-TCs, and to compare the differences. Table 4 indicates the averaged atmospheric environmental parameters at genesis time, mature time, and decay time. In the same manner as oceanic parameters, the average values were calculated for: (1) an annulus average of 200–800 km, and (2) area average within 300 km from the TC center. Another important factor is the VWS because it generally causes the asymmetric convection and suppresses TC genesis and intensity (Frank and Richie, 2001; Maru et el. 2018). Weak VWS is one of the essential atmospheric parameters favorable for TC intensification (Gray,1979 and Wada et al. 2007). The average VWS was significantly weaker in RI-TCs at both genesis time and mature time and significantly, different between RI-TCs and NR-TCs (Table 4). The average VWS values are weaker closer to the TC center within 300 km for both RI-TCs and NR-TCs at genesis time and mature time. The higher values especially with 200–800 km radius shown at decay time (Table 4) is due to strong westerlies in ET transitioning region and poleward tracks (Fig. 1b) where TCs start losing strength due to cooler SST interaction.

Figure 10c reveals the distribution of VWS averaged across the study domain. The VWS averaged over 37 years analysis period 1986–2022 is less than 12 m s^{-1} north of 15°S and becomes stronger towards the south due to the influence of the mid-latitude westerly jet in the western region of the domain (Fig. 10c). This is consistent with RI-TCs genesis locations and explains the influence of weak VWS corresponding to locations of RI-TC cases (Fig. 1). Similarly, higher amplitudes of VWS greater than 12 m s^{-1} are also observed from equator right through poleward and extended beyond longitudes 140°W (220°) in the central and eastern pacific up to 120°W (240°) eastern border of study domain (Fig 10c). Figure 10h shows the difference between RI-TCs and NR-TCs (RI-NR) and generally, VWS is weaker and favorable for development of RI-TCs cases. Figure 11 presents the occurrence rates distribution of area average VWS within 300 km around the TC center for RI-TCs and NR-TCs. The occurrence rate of RI-TCs among distribution of weak VWS (5–10 m s^{-1}) was (53.7%) greater than that of NR-TCs (35.1%). The result indicates that rapid TC intensification invariably generated under weak VWS without being inhibited by the unfavorable environment. Relative humidity between lower and mid-troposphere (RHLO and RHMD) at the genesis time, mature time and decay time did not differ significantly, except that the difference of RHMD is barely significant. The average relative humidity values are higher closer to the TC center (annular ring of 300 km) for both RI-TCs and NR-TCs at genesis time and mature time. Higher RHMD in RI-TCs at the genesis time implies that middle tropospheric moisture is also favorable for development of deep convections, supporting the RI events (Table 4). Figure 10d and 10e reveals the distribution of relative humidity averaged across the study domain respectively for the lower and mid-troposphere (RHLO and RHMD). Figure 10d reveals that RHLO is high (~ 70–80%) south of the equator within the study domain, in particular around the Solomon Islands, Vanuatu, Samoa Fiji, Tonga, French Polynesia and northern regions of Queensland, and New Caledonia. Similarly, higher values of deep moist (~70–80%) are also observed in the RHMD layer from north of 15°S starting at western side of domain and ends at around longitude 200°E in the central pacific (Fig 10e). The results indicated in Fig. 10d and 10e are consistent with RI-TCs genesis locations illustrated in Fig. 1a. Figure 10i and 10j shows very little large-scale difference between RI-TCs and NR-TCs.

Some may wonder the environmental conditions for 1996 and 2008, in which no RI-TC was recorded (Fig. 5b). The oceanic and atmospheric environmental parameters around the TC center were calculated as in Tables 3 and 4. This analysis reveals that lower TCHP in 1996 and 2008 were not favorable for RI-TC occurrence (not shown).

4. Discussion

4.1 Dependency on ENSO phase

Figure 7 showed that the occurrence rate of RI-TC in El Niño years is higher than in La Niña years. It could be explained by the change in the genesis location of TCs because RI-TCs over the SWP basin are mainly concentrated in the low latitude where the climatology is characterized by high SST, relative humidity, and low VWS. Another candidate for the difference is the change in the physical parameters according to the ENSO phase.

First, we investigated the average location for RI-TCs and NR-TCs at genesis time during El Niño, neutral, and La Niña years (Table 5). Figure 12 shows the distribution of RI-TCs according to the ENSO phases, while Fig. 13 illustrates the distribution of all TCs. They reveal that the typical locations of RI-TCs do not change much according to the ENSO phase. Table 5 shows that RI-TCs tend to form northward (13.45°S) than NR-TCs (15.25°S) in El Niño years, same as in La Niña years (13.01°S and 16.46°S for the mean genesis latitude of RI-TCs and NR-TCs, respectively). The shift in the mean TC genesis locations during ENSO years is consistent with the findings of Maru et al., (2018). It is worth mentioning that the mean latitude of the genesis of RI-TCs does not change much regardless of the ENSO phase, while the mean latitude of the genesis of all TCs is much north during the El Niño phase. The northern genesis of all TCs is favorable for higher rate of RI-TCs during El Niño recalling the climatological environment. It should be reminded that the TC genesis is frequently observed around the south pacific convergence zone (SPCZ). Vincent et al.

(2011) stated that the ENSO phenomenon strongly modulates the SPCZ movement, and the enhanced convective activities in the SPCZ region is shown to constrain tropical cyclogenesis to occur preferentially within 10°S.

The composite mean of atmospheric and oceanic environmental conditions at the genesis time of RI-TCs is shown for the El Niño and La Niña phases in Fig. 14. It shows that the thermodynamic conditions are favorable for the RI-TCs around the dateline in the low-latitudes (high SST, high TCHP, and low VWS) during the El Niño phase. The high SST and TCHP indicate the eastward extension of warm pool. In this tropical region, the TCHP is positively correlated to the SST distribution, where the mixing layer is very deep. Previous studies (e.g., Bhowmick et al., 2023) have shown that the influx of warm ocean water to the east of 170°E increases the potential of a higher number of intensifying TCs. Yonekura et al. (2014) described that teleconnection patterns such as ENSO causes a shift in SST towards the west during La Niña years and towards the east during El Niño years. The current study supports the eastward extension of the region favorable for RI-TCs. However, it should be kept in mind that the occurrence rate of RI-TCs is not necessarily high around the dateline in the El Niño phase (Figs. 12 and 13), and the impact is not verified with the current data.

The relationship between the distribution of RI-TCs and the occurrence rates in each ENSO period may be attributed to environmental physical parameters discussed above. However, we did not focus on TCs that made landfall and are left for future works.

4.2 Similarities and differences with other basins

There are notable differences and common aspects of RI-TCs in the SWP with those in other basins. In the SWP, the RI onset tends to commence at 0-6 h after the tropical cyclogenesis, which are much earlier than WNP peaking at 12-24 h after the cyclogenesis (Fig. 5 of Fudeyasu et al. 2018). This reflects that the RI-TC genesis locations in SWP are generally within the RI zone, while RI-TCs in the WNP were not necessarily generated in the RI zone especially during the El Niño period (Fig. 11 of Fudeyasu et al. 2018). Nevertheless, the eastward shift of cyclogenesis in the El Niño period is likely to enhance the possibility of passing the RI zone, which can explain the higher rate of RI-TCs in NWP. The relationship between the genesis location and RI zone is not clear. However, it might be related to the large-scale conditions. The regions with high TCHP, low VWS, and high RH, which are favorable for TC development, heavily overlap in SWP, while they do not in WNP (Fig. 10 of Fudeyasu et al. (2018)). In the common aspects, longer duration of developing period and longer life span for the RI-TCs than for the NR-TCs are found in both the SWP and the WNP (see Fudeyasu et al. 2018). Kaplan and DeMaria (2003) examined the RI-TCs and NR-TCs in the north Atlantic and demonstrated that differences in the SST and VWS are more evident than in humidity. This feature is also true of the WNP TCs (Fudeyasu et al. 2018) and SWP, except for the difference of the marginal mid-tropospheric humidity in the surrounding region at the genesis stage of the TC in the SWP. The El Niño phase for the increasing number of RI-TC has also been identified in the WNP. A higher (lower) occurrence rate of RI-TC in El Niño (La Niña) was observed (Fudeyasu et al. 2018).

5. Conclusions

This study statistically investigates the characteristics of TCs undergoing RI in the SWP and relevant environmental parameters over 37 years from 1986 to 2022. Among the 364 TCs investigated, 82 TCs satisfied the criteria of a maximum wind speed increase of 30 kt or more in a 24-hour period.

RI-TCs preferentially occurred during the southern hemisphere summer/TC season (November to April) with a high variability in seasonality among the number of RI-TCs. RI-TCs commonly occurred during January to March with a peak in March. Analyzing the long-term trends of the annual number of RI-TCs occurrences over the SWP from 1986 to 2022 shows that the frequency of RI-TCs has been slowly increasing. However, the slow increasing trend in the 37-yr period was not statistically significant. On the other hand, the annual number of all TCs (RI-TCs and NR-TCs) analyzed in this study shows a decreasing trend but also not statistically significant. Based on the 10-yr mean of RI-TC occurrence rates from 1986 to 2022. The rates of RI-TC occurrence increased from 1990s to 2020s, with a peak in the 2008-2017 (29%) interval.

The maximum sustained wind speed (central pressure) of RI-TCs was significantly higher (lower) than NR-TCs at mature time. RI-TCs tend to develop into more severe TCs as a result of formation in environments favorable for TC development. The average location of RI-TCs at genesis time shows that, RI-TCs tend to form significantly more northward than NR-TCs. The development stage and lifespan are longer in RI-TCs than NR-TCs.

TCs in El Niño years tended to undergo RI more frequently presumably due to the average genesis location of warm SST to the further north and central pacific. The average number of RI-TCs per year and the average occurrence rate were 2.6 and 26.6% during El Niño years, whereas those were lower in La Niña years (1.8, 17.8%) and neutral years (1.9, 20.2%). The RI onset time is usually 0–42 h peaked at 0–6 h after the genesis time. The RI duration is usually less than 3 days and peaks at 1-day. Interestingly, one event (TC Winston 2016) attained RI duration of 114-h. RI is most frequently observed over the zonally elongated area around coral sea, south of Solomon Islands (Solomon Sea), Vanuatu, Fiji and Samoa (RI zone as at longitudes of 145°E–160°W and latitudes of 8°S–20°S). This is consistent with regions of higher SST, TCHP, weak VWS and deep moist layer.

Average values of SST and TCHP are significantly higher than those of NR-TCs at both genesis and mature times. The average relative humidity between lower and mid-troposphere (RHLO and RHMD) at the genesis time and mature time did not differ significantly but are higher in RI-TCs. The average values for VWS are significantly weaker in RI-TCs at both genesis time and mature time and significantly different between RI-TCs and NR-TCs. The occurrence rate of RI-TCs among distribution of weak VWS (5–10 m s^{-1}) within 300 km around the TC center was (53.7%) greater than that of NR-TCs (35.1%).

These results are meaningful because the general characteristics of RI-TCs around the SWP region were described for the first time and were proved to be consistent with global-scale and/or other basin-scale features. TC RI events has been a great challenge for disaster prevention. They can pose imminent impacts on the region and its local communities. The authors believe that this work will help mitigate and prevent TC-related disasters through improving the prediction skill of RI-TCs in the SWP.

Data Availability Statement

The Southwest Pacific Enhanced Archive for Tropical cyclones (SPEArTC) best track (BT) data are available online on the Asia-Pacific Data-Research Center (APDRC) website. (available at https://apdrc.soest.hawaii.edu/projects/speartc/download_speartc.php, accessed on 22 November 2022). The monthly ENSO indexes were obtained from BoM (available at http://www.bom.gov.au/climate/enso/soi/, accessed on 30 October 2024. The specific humidity, air temperature, geopotential height, zonal and meridional wind datasets were taken from the Japanese 55-year Reanalysis (JRA-55; Kobayashi et al. 2015) (details available online at http://jra.kishou.go.jp/JRA-55/index_en.html). Ocean data, SST was taken from the delayed mode of Merged Satellite and in-situ data Global Daily Sea Surface Temperature (MGDSST) (Kurihara et al. 2006) and TC heat potential (TCHP) was taken from Japan Agency for Marine-Earth Science and Technology (JAMSTEC), Japan Coastal Ocean Predictability Experiments-Forecasting Global Ocean (JCOPE-FGO) on request (Kido et al. 2022)

Acknowledgments

The authors would like to thank the helpful comments from Prof. Tetsuya Takemi. This work was supported by Japan International Cooperation Agency SDG's Global Leaders Program, JSPS KAKENHI JP21H01156 and JP23K26359, and the Program for The Advanced Studies of Climate Change Projection (SENTAN, Grant Number JPMXD0722678534) funded by MEXT.

References

Balaguru, K. G., 2018: Increasing magnitude of hurricane rapid intensification in the central and eastern tropical Atlantic. *Geophys. Res. Lett.,* **45***,* 4238− 4247.

Bhatia, K. T., G. A. Vecchi, ,T. R. Knutson, ,H. Murakami, , J. Kossin, ,K. W Dixon, , & C. E. Whitlock, 2019: Recent increases in tropical cyclone intensification rates. *Nature communications*, **10**, 1-9.

Bhatia, K., A. Baker, W. Yang, G. Vecchi, T. Knutson, H. Murakami, H., ... and C. Whitlock, 2022: A potential explanation for the global increase in tropical cyclone rapid intensification. *Na. Commun.*, **13**, 6626.

Bhowmick, R., J. C. Trepanier, J. C., & A. M. Haberlie, 2023: Classification Analysis of Southwest Pacific Tropical Cyclone Intensity Changes Prior to Landfall. *Atmosphere*, **14**, 253, doi.org/10.3390/atmos14020253.

Bosart, L. F., C. S. Velden, W. E. Bracken, J. Molinari, and P. G. Black, 2000: Environmental influences on the rapid intensification of Hurricane Opal (1995). over the Gulf of Mexico. *Mon. Wea. Rev.,* **128**, 322–352.

Chand, S. S., and K. J. E. Walsh, 2010: The influence of the Madden–Julian oscillation on tropical cyclone activity in the Fiji region. *J. Climate*, **23**, 868–886.

Cione, J. J., and E. W. Uhlhorn, 2003: Sea surface temperature variability in hurricanes: Implications with respect to intensity change. *Mon. Wea. Rev*., **131**, 1783–1796.

Diamond, H. J., A. M. Lorrey, and J. A. Renwick, 2013: A southwest Pacific tropical cyclone climatology and linkages to the El Niño–Southern Oscillation. *J. Climate*, **26**, 3–25.

Diamond, H. J., A. M. Lorrey, K. A. Knapp, and D. H. Levinson, 2012: Development of an enhanced tropical cyclone tracks database for the southwest Pacific from 1840 to 2010. *Int. J. Climatol.,* **32**, 2240–2250.

Emanuel, K.A., 1999: Thermodynamic control of hurricane intensity. *Nature* **401**, 665–669.

Emanuel,K. A., 2005: *Devine wind: The History and Scince of Hurricanes*. Oxford University Press, 285 pp.

Eastin, M. D., W. M. Gray, and P. G. Black, 2005: Buoyancy of convective vertical motions in the inner core of intense hurricanes. Part II: Case studies. *Mon. Wea. Rev.*, **133**, 209–227.

Frank, W. M., and E. A. Ritchie, 2001: Effects of vertical wind shear on the intensity and structure of numerically simulated hurricanes. Mon. Wea. Rev., 1**29**, 2249–2269.

Fudeyasu, H., K. Ito, and Y. Miyamoto, 2018: Characteristics of tropical cyclone rapid intensification over the western North Pacific. *J. Climate*, **31**, 8917–8930.

Gray, W. M. 1979: Hurricanes: Their formation, structure and likely role in the tropical circulation. Meteorology over the tropical oceans. *Roy. Meteor. Soc.*, 155–218.

Haruhiru, A., S. S. Chand, C. Turville, and H. Ramsay, 2023: Tropical cyclone activity in the Solomon Islands region: Climatology, variability, and trends. *Int.J. Climatol.*, **43**, 593–614.

Ito, K., 2016: Errors in tropical cyclone intensity forecast by RSMC Tokyo and statistical correction using environmental parameters. *SOLA*, **12**, 247–252.

Kaplan, J., and M. DeMaria, 2003: Large-scale characteristics of rapidly intensifying tropical cyclones in the North Atlantic basin. *Wea. Forecasting*, **18**, 1093–1108.

Kaplan, J., M. DeMaria, and J. A. Knaff, 2010: A revised tropical cyclone rapid intensification index for the Atlantic and eastern North Pacific basins. *Weather and forecasting*, **25**, 220–241.

Kido, S., M. Nonaka, and Y. Miyazawa, 2022. JCOPE-FGO: an eddy-resolving quasi-global ocean reanalysis product. *Ocean Dynamics*, ***72***, 599–619.

Kieper, M., and H. Jiang, 2012: Predicting tropical cyclone rapid intensification using the 37 GHz ring pattern identified from passive microwave measurements. *Geophys. Res. Lett.* **39**, L1 3804, doi:10.1029/2012GL052115.

Kieu, C.Q., V. Tallapragada, and W. Hogsett, 2014: Vertical structure of tropical cyclones at onset of the rapid intensification in the HWRF model, *Geophys. Res. Lett.*, **41**, 3298–3306.

Kobayashi, S., Y. Ota, Y. Harada, A. Ebita, M. Moriya, H. Onoda, K. Onogi, H. Kamahori, C. Kobayashi, H. Endo, K. Miyaoka, and K. Takahashi, 2015: The JRA-55 reanalysis: General specifications and basic characteristics. *J. Meteor. Soc. Japan. Ser. II*, **93**, 5–48.

Kranthi, G. M., M. Deshpande, K. Sunilkumar, R. Emmanuel, and S. Ingle, 2023: Climatology and characteristics of rapidly intensifying tropical cyclones over the North Indian Ocean. *Int.J. Climatol*, **43**, 1773–1795.

Kurihara, Y., T. Sakurai, and T. Kuragano, 2006: Global daily sea surface temperature analysis using data from satellite microwave radiometer, satellite infrared radiometer and in-situ observations (in Japanese). *Weather service bulletin*, **73**, S1-18.

Leipper, D. F., and D. Volgenau, 1972: Hurricane heat potential of the Gulf of Mexico. *J. Phys. Oceanogr.*, **2**, 218–224.

Lin, I.-I., C.-H. Chen, I.-F. Pun, W. T. Liu, and C.-C. Wu, 2009: Warm ocean anomaly, air sea fluxes, and the rapid intensification of tropical cyclone Nargis (2008), *Geophys. Res. Lett.,* **36**, L03817, https://doi.org/10.1029/2008GL035815.

Lin, I.-I., C.-C. Wu, K. A. Emanuel, I. H. Lee, C. R. Wu, and I.-F. Pun, 2005: The interaction of Supertyphoon Maemi (2003) with a warm ocean eddy. *Mon.Wea.Rev.*, **133**(9), 2635–2649.

Lin, I.-I., I.-F. Pun, and C. -C. Lien, C. C. 2014: “Category-6” supertyphoon Haiyan in global warming hiatus: Contribution from subsurface ocean warming. *Geophys.Res. Lett.*, **41**, 8547–8553.

Lin, I.-I., C.-C. Wu, I. F. Pun, and D.-S. Ko, 2008: Upper-ocean thermal structure and the western North Pacific category 5 typhoons. Part I: Ocean features and the category 5 typhoons’ intensification. *Mon. Wea. Rev.*, **136**, 3288–3306.

Maru, E., T. Shibata, and K. Ito, 2018: Statistical analysis of tropical cyclones in the Solomon Islands. *Atmosphere*, **9**, 227.

Molinari, J., D. Vollaro, 2010: Rapid Intensification of a Sheared Tropical Storm. *Mon. Wea. Rev.*, **138**, 3869–3885.

Nakano, M., H. Kubota, T. Miyakawa, T. Nasuno, and M. Satoh, M. 2017: Genesis of super cyclone Pam 2015. modulation of low-frequency large-scale circulations and the Madden–Julian oscillation by sea surface temperature anomalies. *Mon. Wea. Rev.*, **145**, 3143–3159.

Nasuno, T., H. Yamada, M. Nakano, H. Kubota, M. Sawada, and R. Yoshida, 2016: Global cloud-permitting simulations of Typhoon Fengshen (2008). Geoscience Letters, **3**, 1-13.

Obasi, G. O. P, 1994: WMO's role in the international decade for natural disaster reduction. *Bull. Amer. Meteor. Soc.*, **75**, 1655–1661.

Rappaport, E. N., J. G. Jiing, C. W. Landsea, S. T. Murillo, and J. L. Franklin, 2012: The Joint Hurricane Test Bed: Its first decade of tropical cyclone research-to-operations activities reviewed. *Bulletin of the American Meteorological Society*, **93**, 371–380.

Shay, L. K., G. J. Goni, and P. G. Black, 2000: Effects of a warm oceanic feature on Hurricane Opal. *Mon. Wea. Rev.,* **128**, 1366–1383.

Shimada, U., M. Yamaguchi, and S. Nishimura, 2020: Is the number of tropical cyclone rapid intensification events in the western North Pacific increasing? *SOLA*, *16*, 1–5.

Smith, R. K., G. Kilroy, and M. T. Montgomery, 2015: Why do model tropical cyclones intensify more rapidly at low latitudes? *J. Atmos. Sci.*, **72**, 1783–1804.

Takemi, T., 2018: The evolution and intensification of Cyclone Pam (2015) and resulting strong winds over the southern Pacific islands. *Journal of Wind Engineering and Industrial Aerodynamics*, 27–36.

Tauvale, L., and K. Tsuboki, 2019: Characteristics of tropical cyclones in the Southwest Pacific. *J..Mete. Soc. Japan. Ser. II*, **97**, 711–731.

Terry, J. P., and A. A. Lau, 2018: Magnitudes of nearshore waves generated by tropical cyclone Winston, the strongest landfalling cyclone in South Pacific records. Unprecedented or unremarkable. *Sedimentary Geology*, **364**, 276–285.

Tu'uholoaki, M., A. Singh, A. Espejo, S. Chand, and H. Damlamian, 2022: Tropical cyclone climatology, variability, and trends in the Tonga region, Southwest Pacific. *Weather Clim. Extrem*, **37**, 100483 https://doi.org/10.1016/j.wace.2022.100483.

Vincent, E.M., M. Lengaigne, C. E. Menkes, N. C. Jourrdain, P. Marchesiello, and G. Madec, 2011: Interannual variability of the South Pacific convergence zone and implications for tropical cyclone genesis. *Clim. Dyn*, **36**, 1881–1896.

Wada, A, 2015: Verification of tropical cyclone heat potential for tropical cyclone intensity forecasting in the Western North Pacific. *Journal of oceanography*, **71**, 373–387.

Wada, A., and N. Usui, 2007: Importance of tropical cyclone heat potential for tropical cyclone intensity and intensification in the western North Pacific. *Journal of Oceanography*, **63**, 427–447.

Wu, C. C., C. Y. Lee, and I.-I. Lin, 2007: The effect of the ocean eddy on tropical cyclone intensity. *J. Atmos. Sci.*, **64**, 3562–3578.

Yonekura, E., and T. M. Hall, 2014: ENSO effect on East Asian tropical cyclone landfall via changes in tracks and genesis in a statistical model. *Journal of Applied Meteorology and Climatology*, **53**, 406–420.

List of Figures

number of RI-TC formed during each ENSO condition, (blue) La Niña, (red) El Niño and (grey) Neutral.

Fig. 6. Yearly total number of all the 364 TCs over the 37-yr analysis period. Regression for each dataset is represented by the thin straight line.

Fig. 7. All TC occurrence in each ENSO condition over the 37-yr analysis period. Blue (orange) color indicates NR-TC (RI-TC) and the numbers inside the bar graphs indicate number of TCs for each ENSO period. The numbers outside the bar graphs indicate the occurrence rates for RI-TCs in each ENSO period.

Fig. 8. Occurrence rates of (a) RI onset time from time of genesis and (b) RI duration between RI onset and RI end time over the 37-yr analysis period.

Fig. 9. Occurrence rates of RI-TCs and NR-TCs divided by the number of severe TCs (category 3–5 TCs) and weak TCs (category 1–2 TCs) over the 37-yr analysis period. Orange bar indicates RI-TCs.

Fig. 10. Composite in large-scale environmental variables for RI-TC at genesis time over the 37-yr analysis period: (a) SST (°C), (b) TCHP ($\mathrm{kJ\ cm^{-2}}$), (**c**) VWS (m s^{-1}), (d) RHLO (%) and

(e) RHMD (%). Panels (f-j) are the same as (a-e) but for difference between RI-TC and NR-TC (RI-TC minus NR-TC). For presentation purpose, XX°W is represented as 360-XX in the longitudinal axis.

Fig. 11. Occurrence rates (%) distribution of area average VWS ($\mathrm{m\,s^{-1}}$) within 300 km around the TC center for NR-TC (RI-TC) in blue (orange) color.

Fig. 12. Same as in Fig. 1 but for the distribution of RI-TC genesis locations during (a) El Niño, (b) La Niña, and (c) Neutral.

Fig. 13. Same as in Fig. 1 but for the distribution of all TCs genesis location during (a) El Niño, and (b) La Niña years. The rectangular dashed red box indicates the RI zone.

Fig. 14. Composite in large-scale environmental variables for RI-TC at genesis time during El Niño years over the 37-yr analysis period: (a) SST (°C), (b) TCHP ($\mathrm{kJ\,cm^{-2}}$), (c) VWS (m s^{-1}), (d) RHLO (%) and (e) RHMD (%). Panels (f–j) are the same as (a–e) but for La Niña periods. Panels (k–o) are the same as (a–e) but for difference between El Niño and La Niña periods, (El Niño - La Niña). For presentation purpose, XX°W is represented as 360-XX in the longitudinal axis.

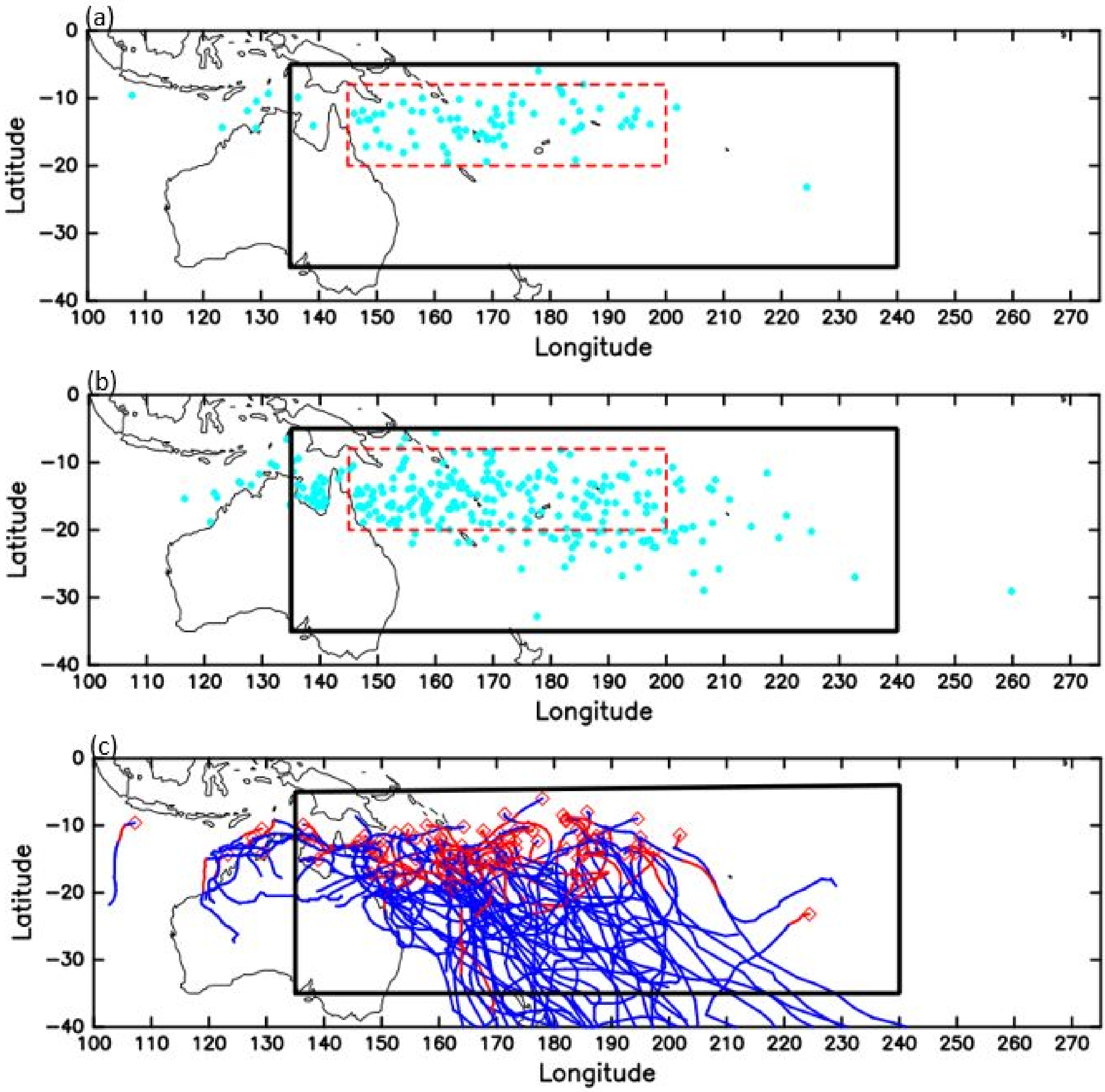

Fig. 1. (a) RI-TC genesis locations (cyan dots), inner red dashed box area indicates the RI zone (longitudes of 145°E –160°W latitudes of 8–20°S) and (b) NR-TC genesis locations (cyan dots). (c) Tracks (red lines) indicates the period of RI for all 82 RI-TCs detected in this study and blue lines indicate the other period. A red diamond indicates RI-TC genesis location same as cyan dots in (a). For presentation purpose, XX°W is represented as 360-XX in the longitudinal axis.

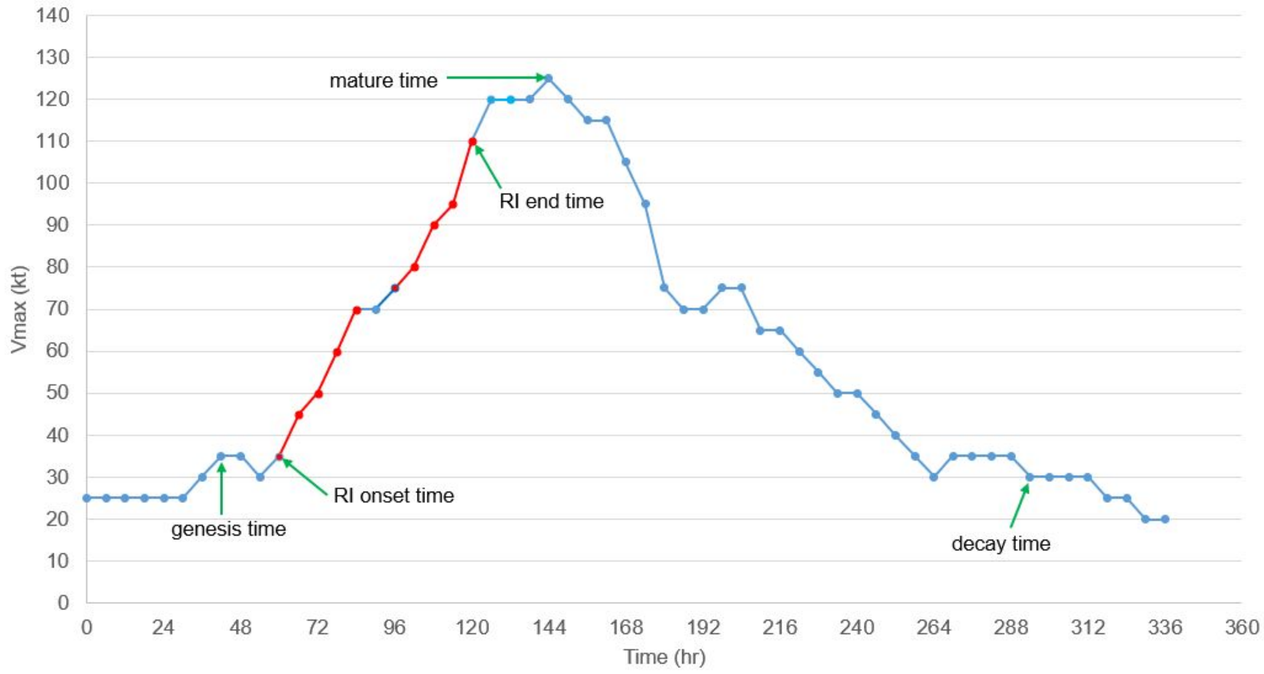

Fig. 2. Maximum wind speed (kt) versus time (h) graph (TC Yasa 12th December 2020) illustrating how RI event is defined using the RI definition and different development stages used in this study. The dots represent the 6-hr observation times. The red (blue) line indicates RI duration (not satisfying RI definition).

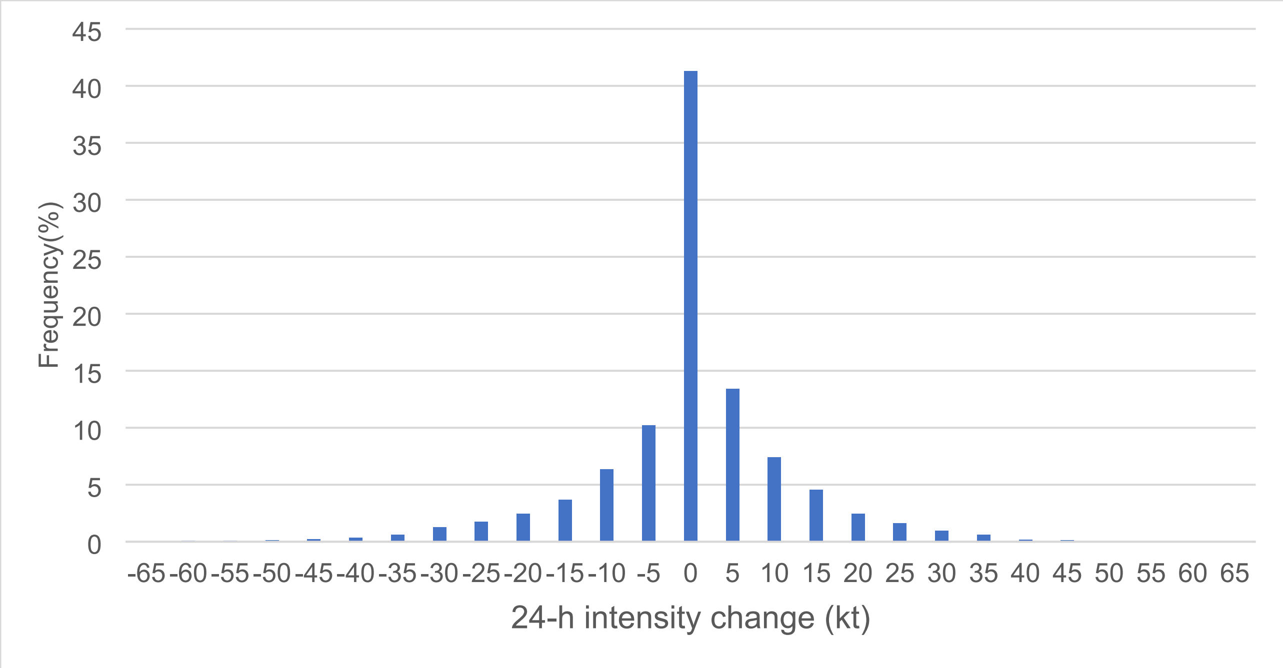

Fig. 3. Frequency distributions of 24-h intensity changes of the 364 TCs over the 37-yr analysis period.

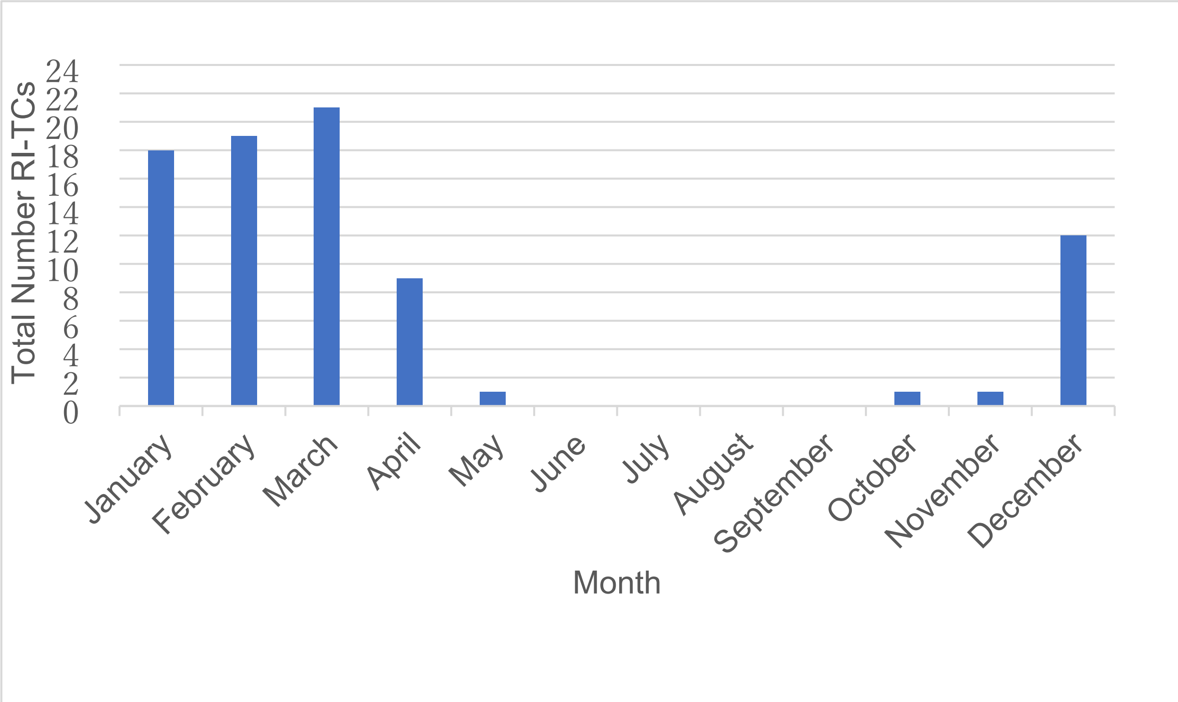

Fig. 4. Monthly total number of RI-TC occurrences over the 37-yr analysis period.

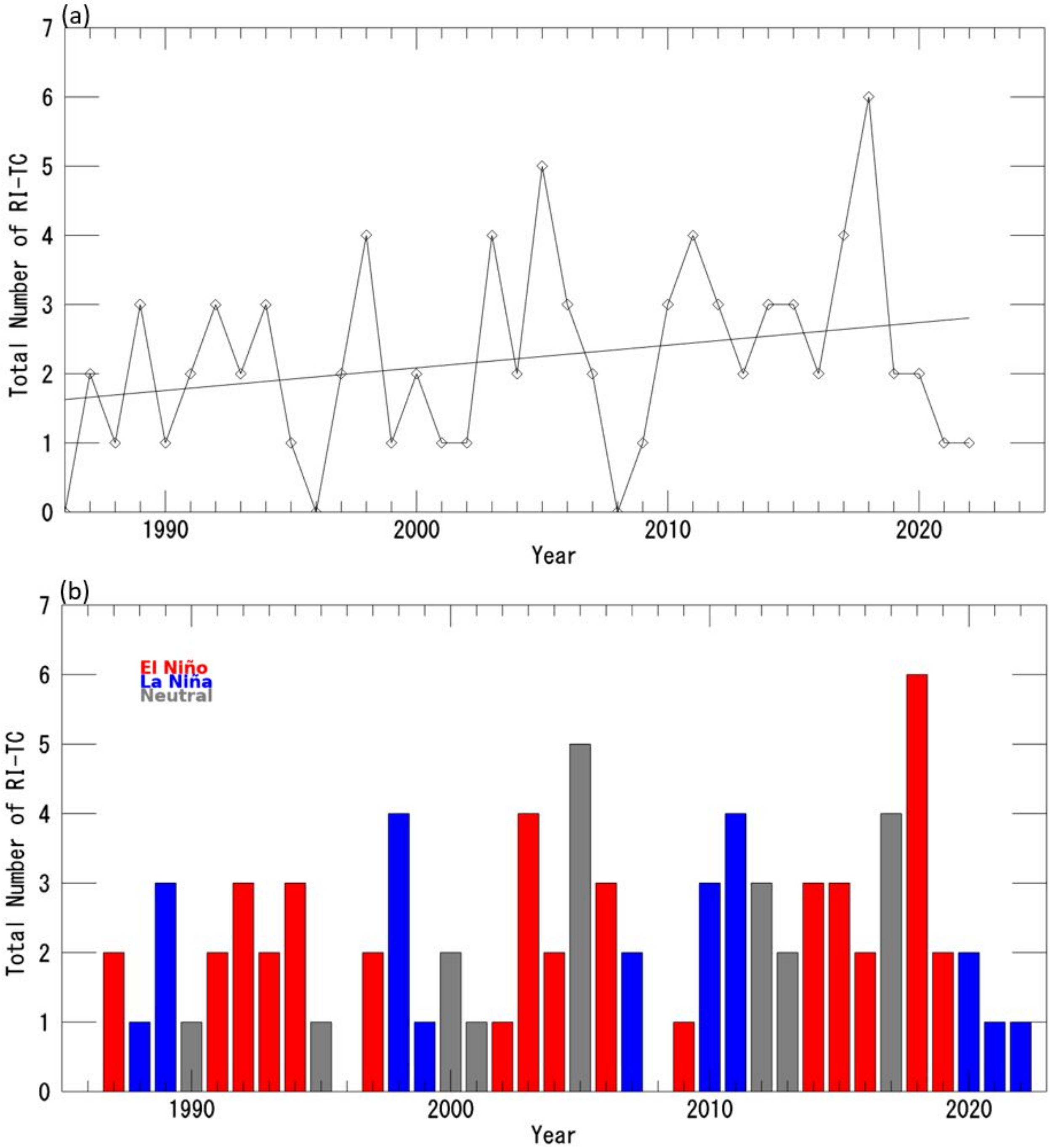

Fig. 5. (a) Number of RI-TC occurrences per year over the 37-yr analysis period. Regression for each dataset is represented by a thin line. (b) the same as (a), except it shows the total number of RI-TC formed during each ENSO condition, (blue) La Niña, (red) El Niño and (grey) Neutral.

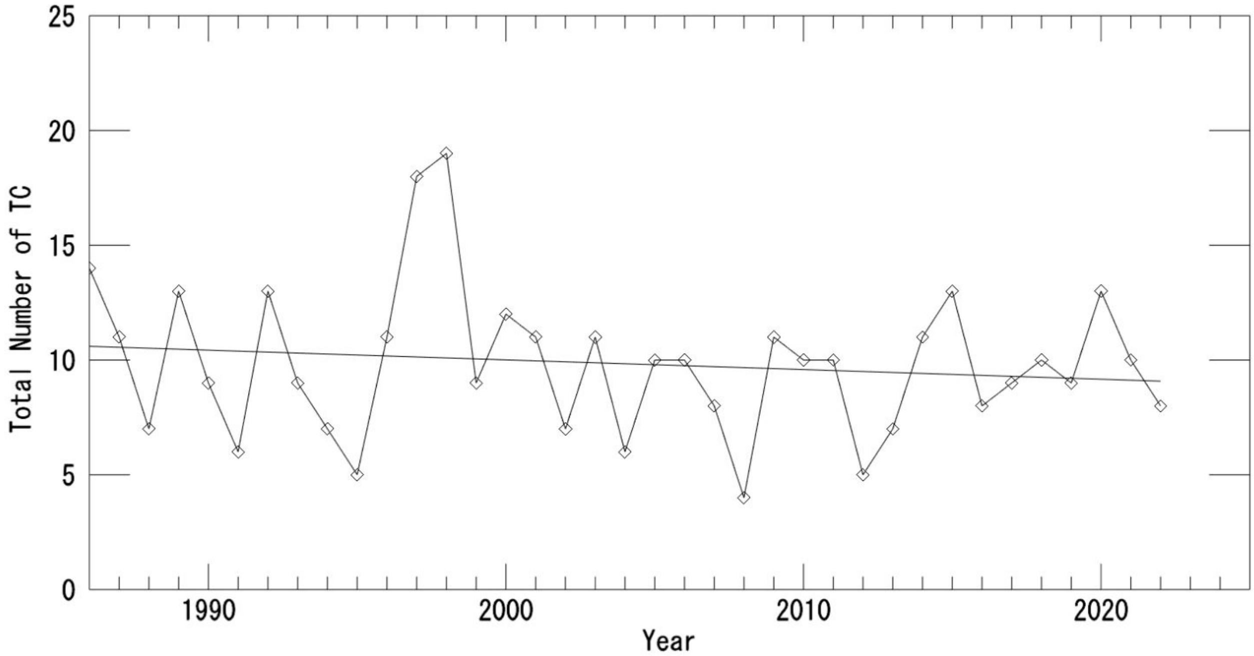

Fig. 6. Yearly total number of all the 364 TCs over the 37-yr analysis period. Regression for each dataset is represented by the thin straight line.

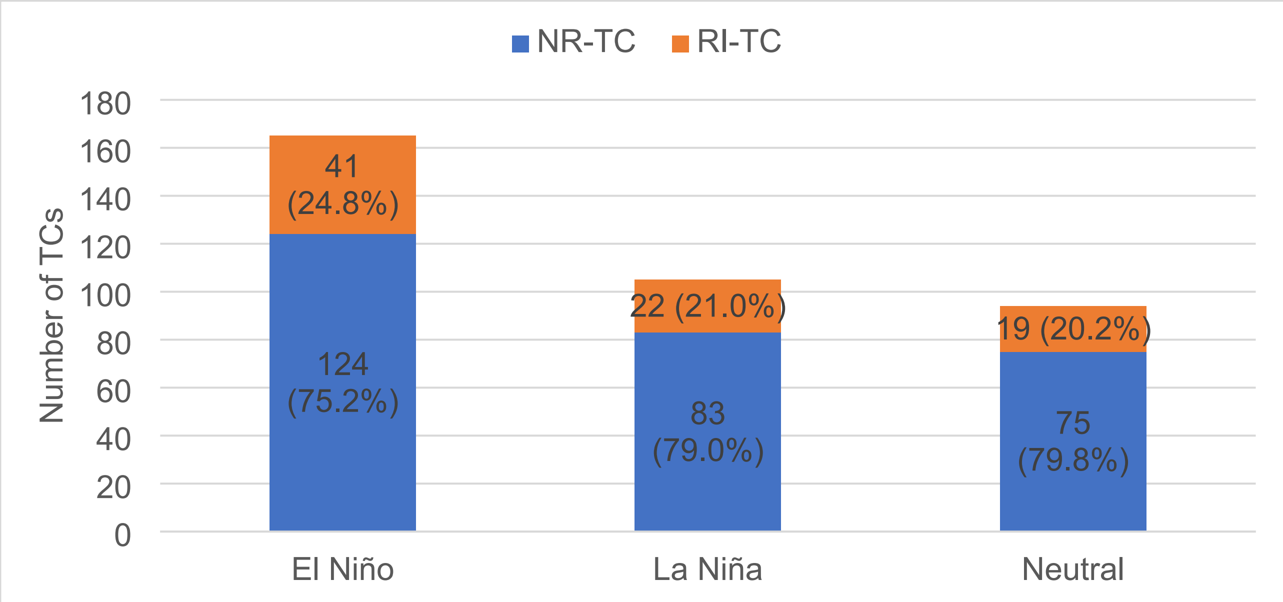

Fig. 7. All TC occurrence in each ENSO condition over the 37-yr analysis period. Blue (orange) color indicates NR-TC (RI-TC) and the numbers inside the bar graphs indicate number of TCs for each ENSO period. The numbers outside the bar graphs indicate the occurrence rates for RI-TCs in each ENSO period.

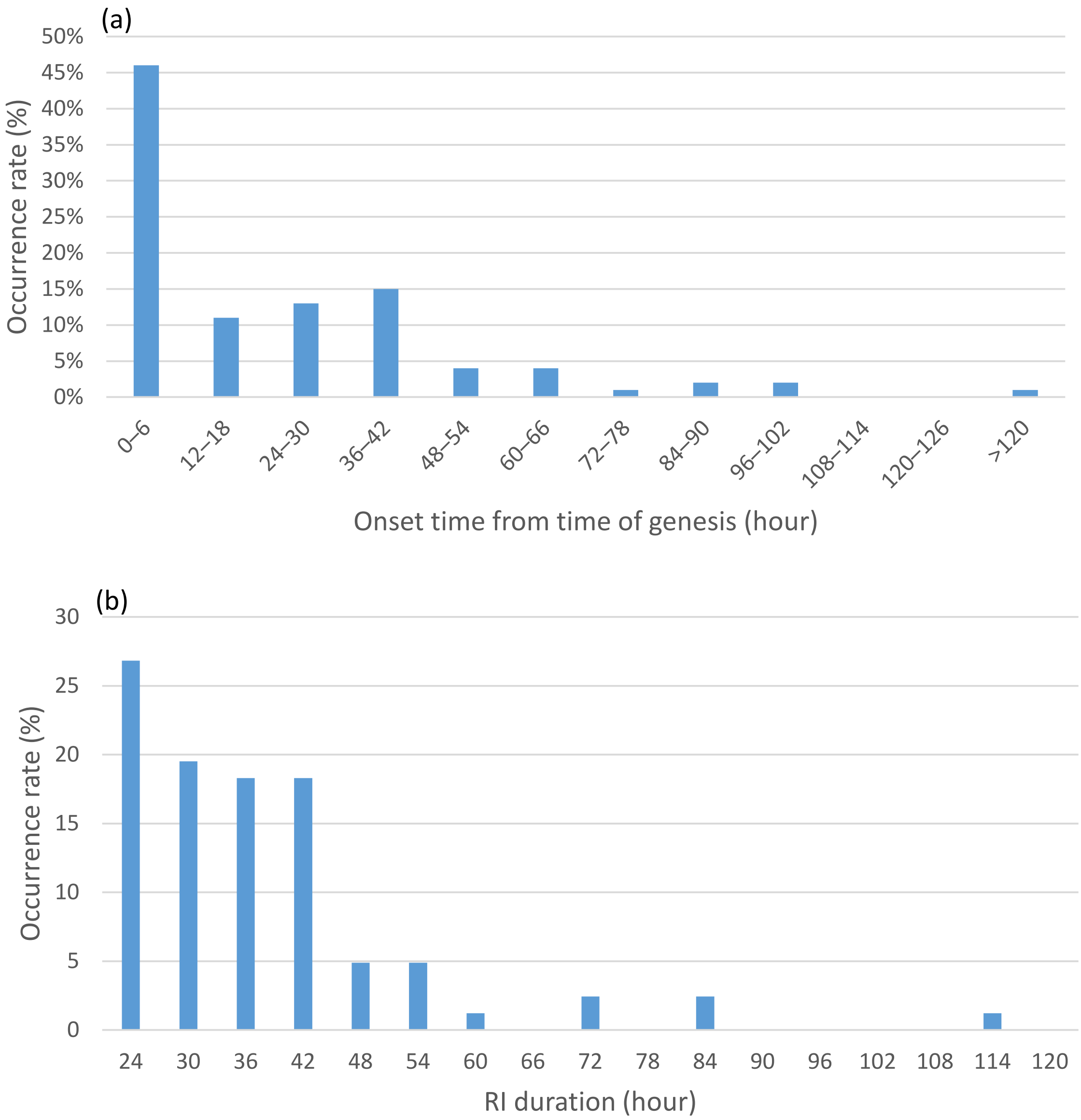

Fig. 8. Occurrence rates of (a) RI onset time from time of genesis and (b) RI duration between RI onset and RI end time over the 37-yr analysis period.

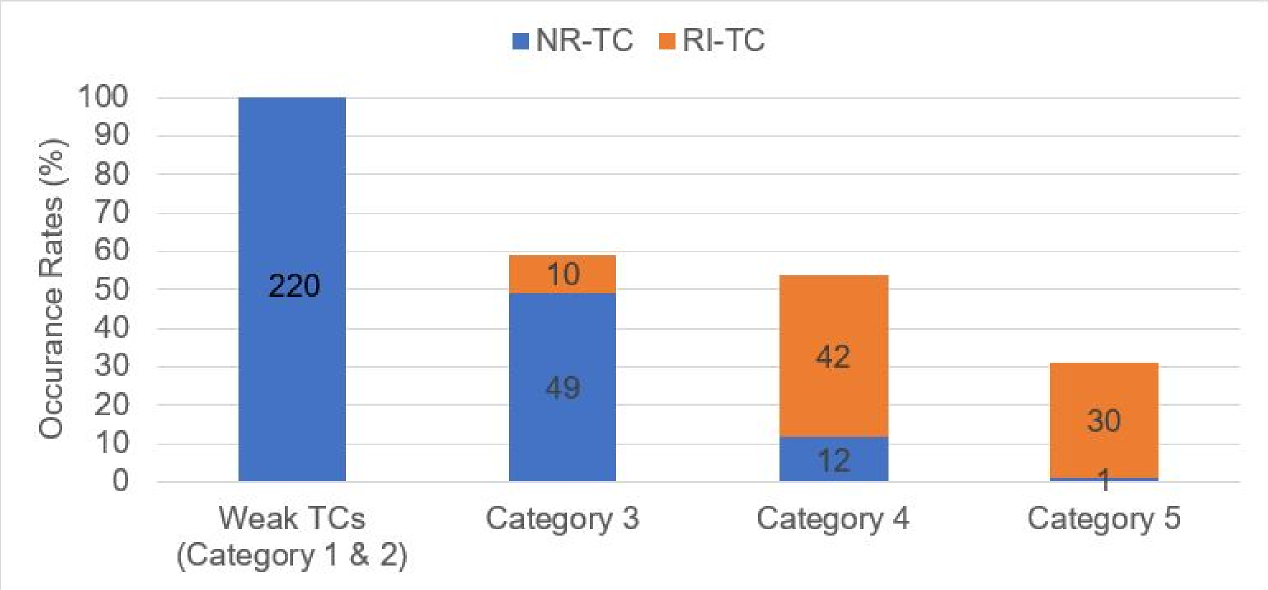

Fig. 9. Occurrence rates of RI-TCs and NR-TCs divided by the number of severe TCs (category 3–5 TCs) and weak TCs (category 1–2 TCs) over the 37-yr analysis period. Orange bar indicates RI-TCs.

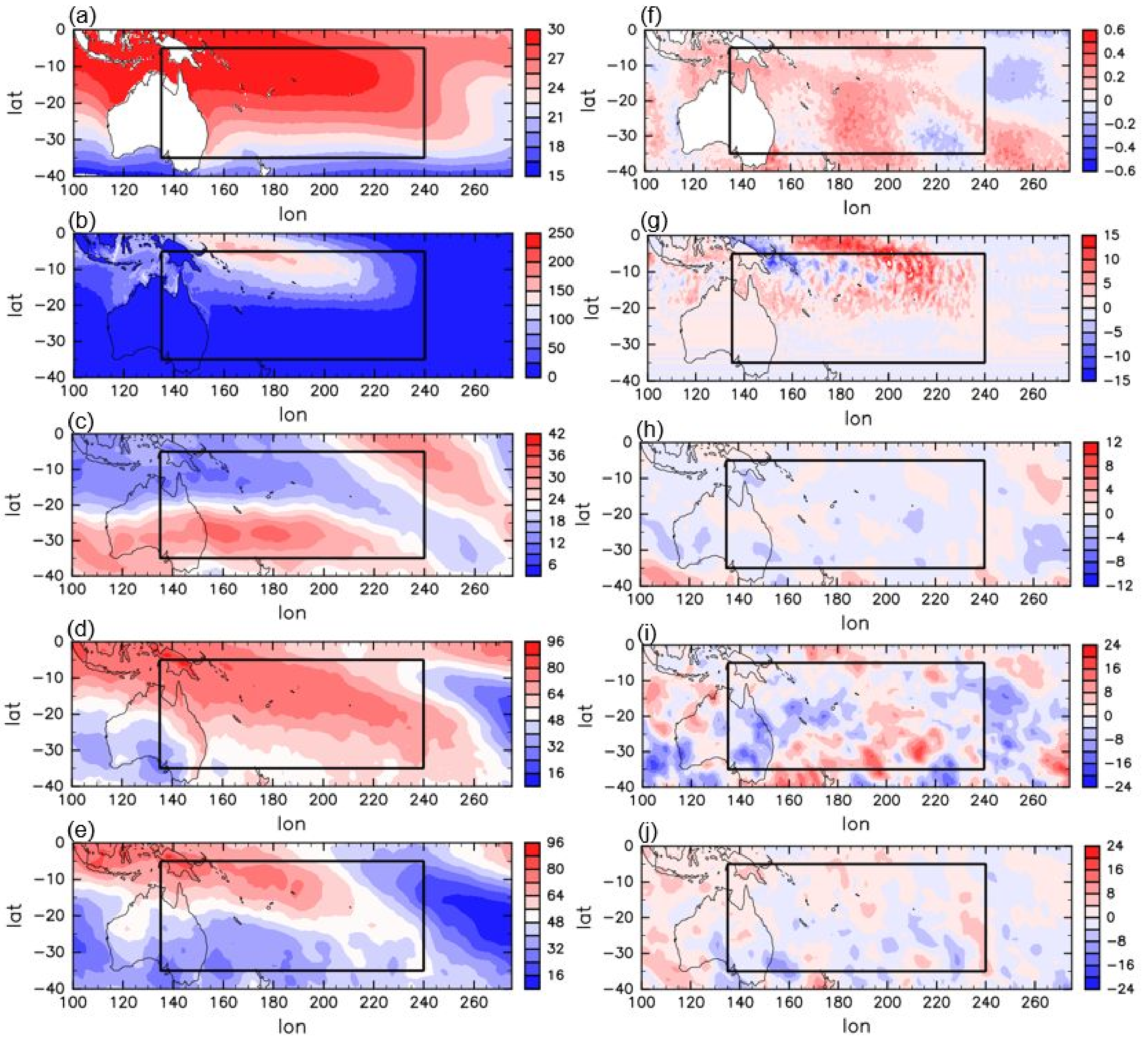

Fig. 10. Composite in large-scale environmental variables for RI-TC at genesis time over the 37-yr analysis period: (a) SST (°C), (b) TCHP ($\mathrm{kJ\ cm^{-2}}$), (**c**) VWS (m s^{-1}), (d) RHLO (%) and (e) RHMD (%). Panels (f-j) are the same as (a-e) but for difference between RI-TC and NR-TC (RI-TC minus NR-TC). For presentation purpose, XX°W is represented as 360-XX in the longitudinal axis.

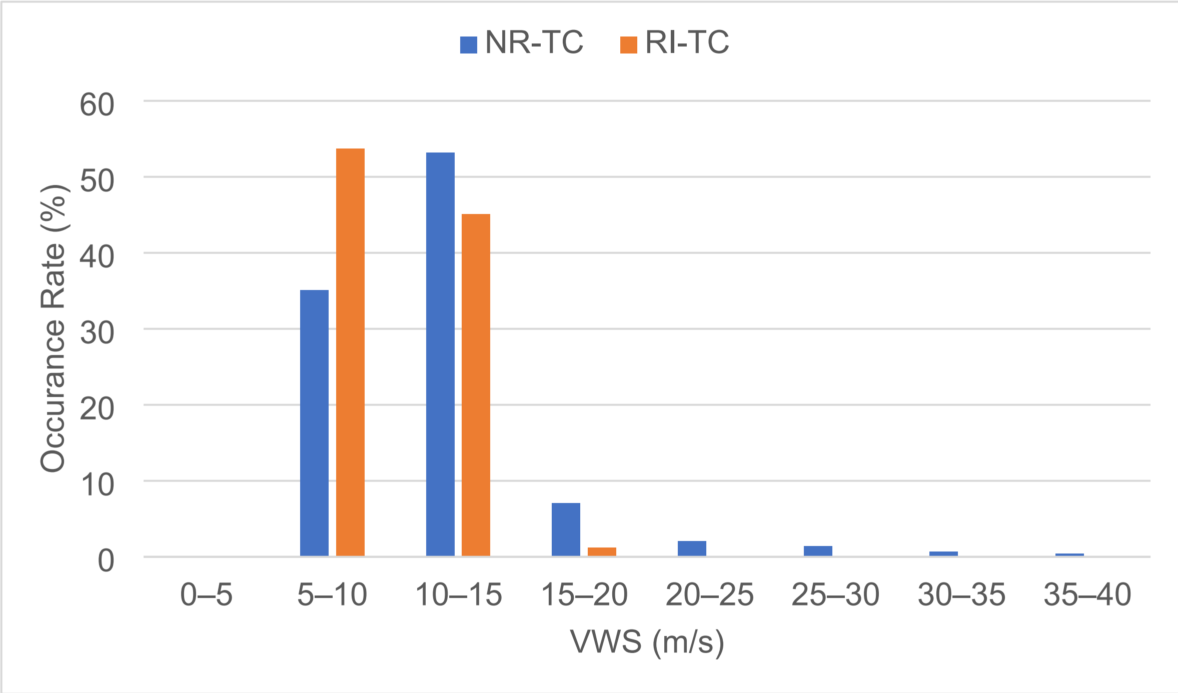

Fig. 11. Occurrence rates (%) distribution of area average VWS ($\mathrm{m\,s^{-1}}$) within 300 km around the TC center for NR-TC (RI-TC) in blue (orange) color.

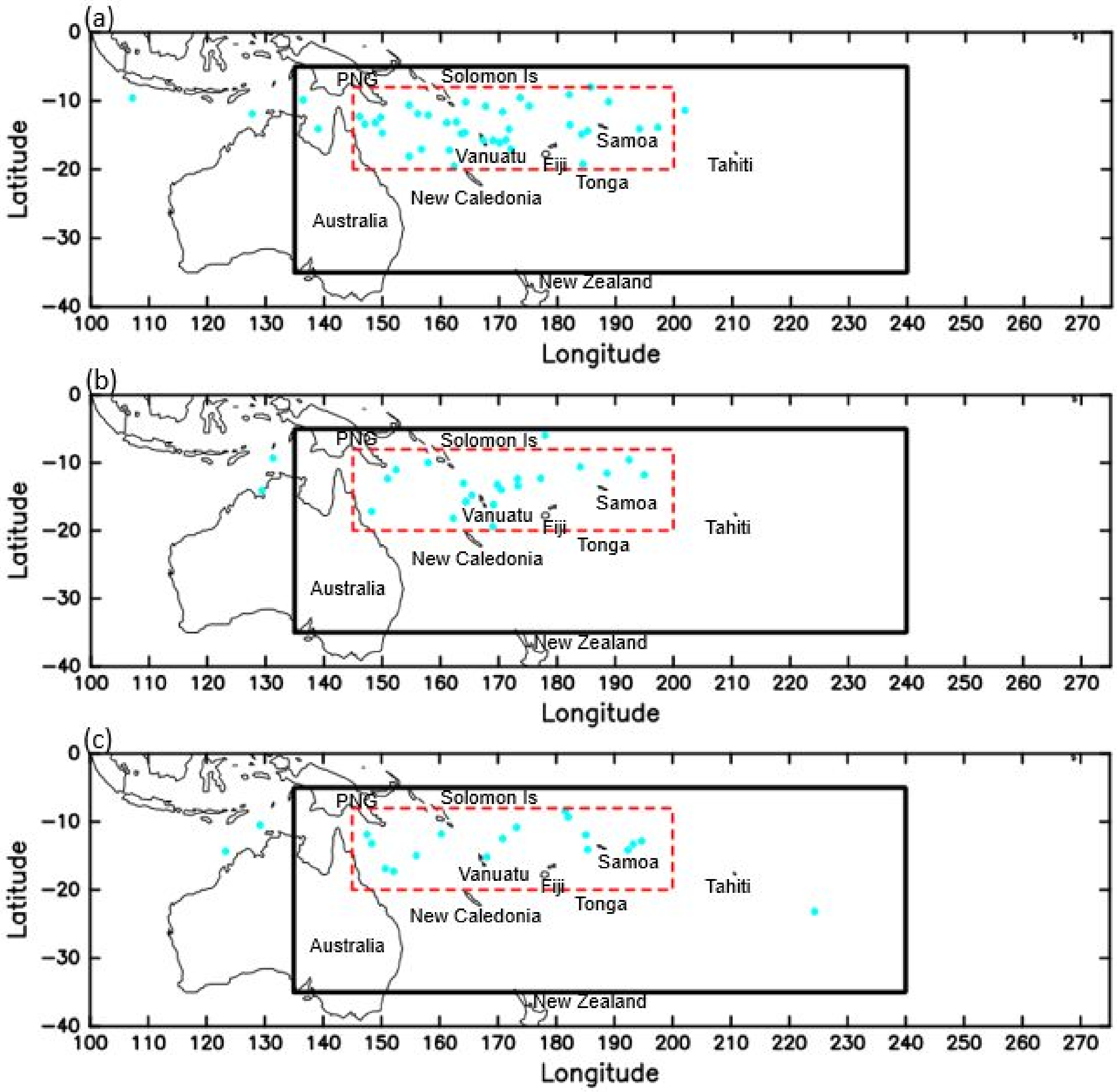

Fig. 12. Same as in Fig. 1 but for the distribution of RI-TC genesis locations during (a) El Niño, (b) La Niña and (c) Neutral.

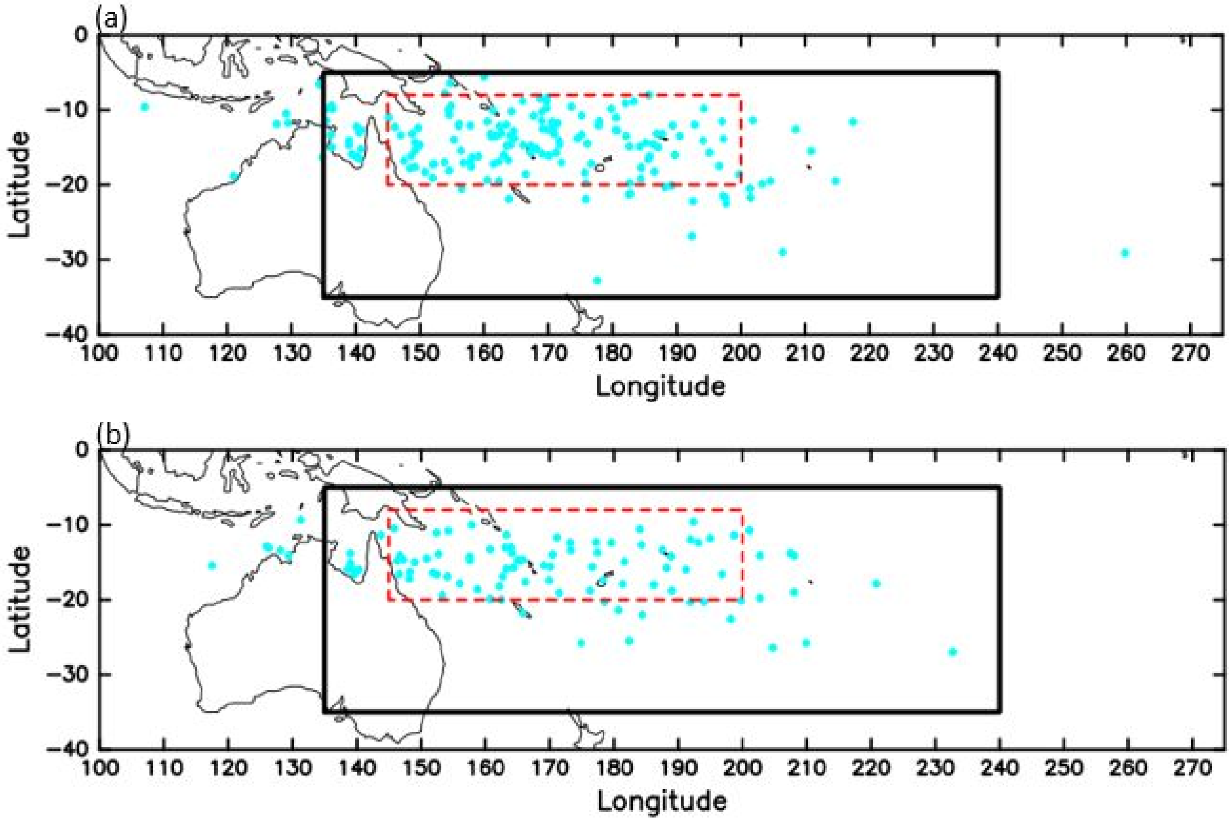

Fig. 13. Same as in Fig. 1 but for the distribution of all TCs genesis location during (a) El Niño, and (b) La Niña years. The rectangular dashed red box indicates the RI zone.

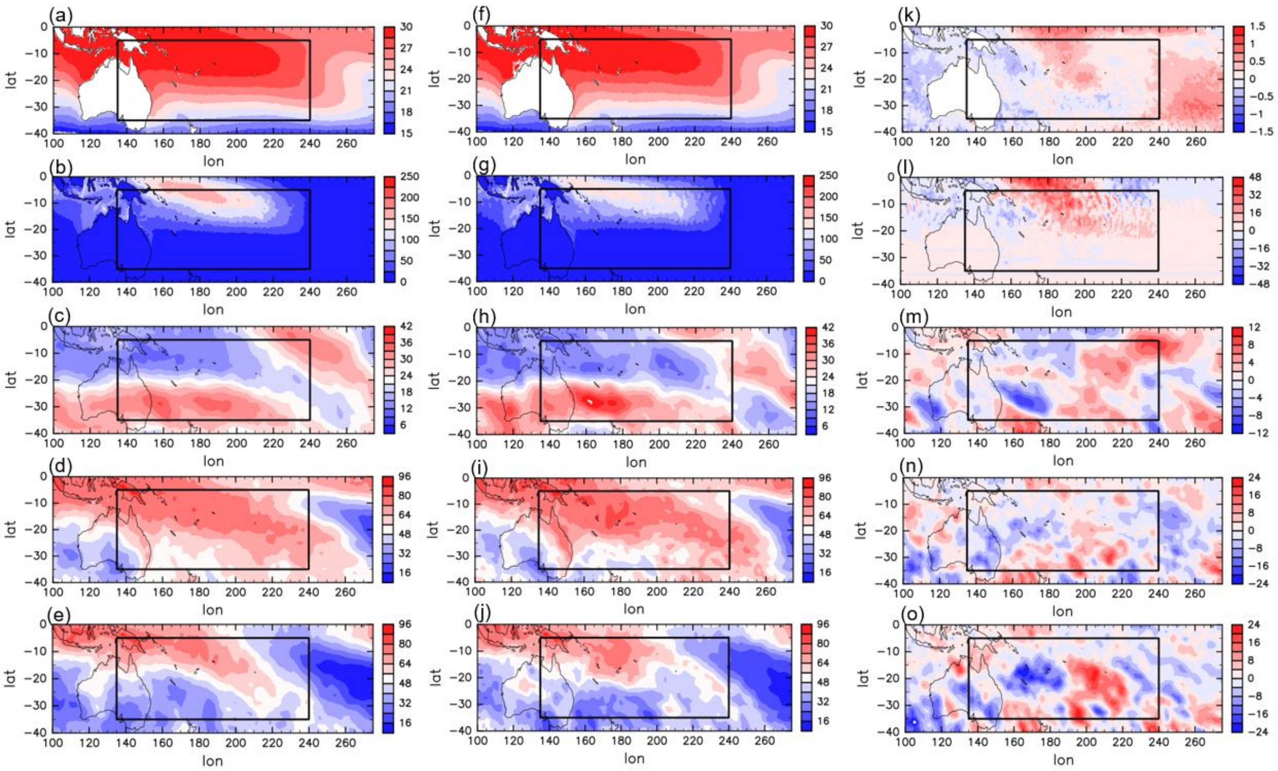

Fig. 14. Composite in large-scale environmental variables for RI-TC at genesis time during El Niño years over the 37-yr analysis period: (a) SST (°C), (b) TCHP (kJ cm^{-2}), (c) VWS (m s^{-1}), (d) RHLO (%) and (e) RHMD (%). Panels (f–j) are the same as (a–e) but for La Niña periods. Panels (k–o) are the same as (a–e) but for difference between El Niño and La Niña periods, (El Niño - La Niña). For presentation purpose, XX°W is represented as 360-XX in the longitudinal axis.

List of Tables

Table 1. Frequency of occurrence of RI-TCs and NR-TCs, and their respective rates of occurrence. Data are classified into 10-yr intervals except the last interval is only 5-yr.

Table 2. Statistical summary of Characteristics of RI-TCs and NR-TCs and their sum (ALL),

over the 37-yr analysis period. If differences from grand means are statistically significant at the 95% confidence level in a two-tailed *t*-test, the values are marked in italics red.

Table 3. Statistical summary of oceanic environmental physical parameters around RI-TCs (RI) and NR-TCs (NR), and their sum (All), over the 37-yr analysis period. If differences from grand means are statistically significant at the 95% confidence level in a two-tailed *t*-test, the values are marked in italics red. The numbers in parentheses are the differences calculated at 0-300 km around the TC center and non-parenthesis numbers indicate differences calculated at 200-800 km around the TC center.

Table 4. As in Table 3, but for environmental physical parameters around RI-TCs and NR-TCs, and their sum (All), over the 37-yr analysis period.

Table 5. Statistical summary of average latitudes and longitudes for RI-TCs, NR-TCs and all TCs during each ENSO period over the 37-yr analysis period. If differences from grand means are statistically significant at the 95% confidence level between RI-TCs and NR-TCs in a two-tailed *t*-test, the values are marked in italics red. For taking the longitude mean, XX°W was converted to 360-XX.

Table 1. Frequency of occurrence of RI-TCs and NR-TCs, and their respective rates of occurrence. Data are classified into 10-yr intervals except the last interval is only 5-yr.

Interval	RI	NR	RI rate (%)
1986-1995	18	76	19
1996-2005	21	92	19
2006-2015	17	66	20
2016-2022	26	48	35

Table 2. Statistical summary of Characteristics of RI-TCs and NR-TCs and their sum (ALL), over the 37-yr analysis period. If differences from grand means are statistically significant at the 95% confidence level in a two-tailed *t*-test, the values are marked in italics red. For presentation purpose, XX°W is represented as 360-XX in the longitudinal axis.

		RI	NR	ALL
	Number	82	282	364
Genesis time	Average lat (°S)	*13.32*	*15.96*	15.37
	Average lon (°E)	166.41	169.20	168.57
Mature time	Duration from genesis time (day)	*3.31*	*1.62*	2.00
	Maximum wind (kt)	*101.28*	*55.33*	66.22
	Minimum pressure (hPa)	*934.78*	*978.57*	971.09
Decay time	Average lat (°S)	*31.13*	*25.02*	26.40
	Average lon (°E)	177.23	174.80	175.37
	Duration from genesis time (day)	*7.86*	*3.72*	4.65

Table 3. Statistical summary of oceanic environmental physical parameters around RI-TCs (RI) and NR-TCs (NR), and their sum (All), over the 37-yr analysis period. If differences from grand means are statistically significant at the 95% confidence level in a two-tailed *t*-test, the values are marked in italics red. The numbers without parentheses are the differences calculated at 200-800 km around the TC center, while the numbers in parentheses are the differences calculated at 0-300 km around the TC center.

		RI	**NR**	**ALL**
Genesis time	SST (°C)	*29.03 (29.10)*	*28.30 (28.40)*	28.47 (29.79)
	TCHP ($kJ\ cm^{-2}$)	*70.75 (73.06)*	*50.93 (50.81)*	55.70 (56.16)
Mature time	SST (°C)	*28.06 (28.12)*	*27.52 (27.58)*	27.64 (27.70)
	TCHP ($kJ\ cm^{-2}$)	*44.23 (44.77)*	*34.65 (31.12)*	36.96 (34.42)
Decay time	SST (°C)	*21.87 (19.75)*	*24.70 (24.41)*	24.07 (23.36)
	TCHP ($kJ\ cm^{-2}$)	*11.23 (7.76)*	*19.71 (14.97)*	17.66 (13.22)

Table 4. As in Table 3, but for environmental physical parameters around RI-TCs and NR-TCs, and their sum (All), over the 37-yr analysis period.

		RI	**NR**	**ALL**
Genesis time	RHLO (%)	79.53 (85.06)	78.57 (85.89)	78.45 (85.70)
	RHMD (%)	*73.19* (83.77)	*71.19* (83.42)	71.64 (83.50)
	VWS ($m\ s^{-1}$)	*13.02 (9.8)*	*16.76 (11.74)*	15.92 (11.34)
Mature time	RHLO (%)	77.57 (87.89)	77.45 (87.09)	77.48 (87.27)
	RHMD (%)	69.56 (87.18)	69.02 (85.17)	69.14 (85.62)
	VWS ($m\ s^{-1}$)	*16.63* (12.88)	*18.68* (13.77)	18.22 (13.57)
Decay time	RHLO (%)	73.33 (88.18)	74.06 (86.34)	73.90 (86.75)
	RHMD (%)	60.20 (75.11)	62.82 (75.68)	62.23 (75.55)
	VWS ($m\ s^{-1}$)	22.53 *(20.00)*	21.36 *(17.87)*	21.62 (18.35)

Table 5. Statistical summary of average latitudes and longitudes for RI-TCs, NR-TCs and all TCs during each ENSO period over the 37-yr analysis period. If differences from grand means are statistically significant at the 95% confidence level between RI-TCs and NR-TCs in a two-tailed *t*-test, the values are marked in italics red. For taking the longitude mean, XX°W was converted to 360-XX.

ENSO Phase		**RI**	**NR**	**ALL**
El Niño	Average lat (°S)	*13.45*	*15.25*	14.78
	Average lon (°E)	164.13	170.11	168.66
Neutral	Average lat (°S)	13.41	16.59	15.95
	Average lon (°E)	172.44	166.27	167.52
La Niña	Average lat (°S)	*13.01*	*16.46*	15.83
	Average lon (°E)	166.64	170.51	169.98